Non-contact Energy Flux Measurement of Impact Pile Driving

Peter C. Meijers[1(✉)] and Francesca Greco[1,2]

[1] Delft University of Technology, Delft, The Netherlands
{p.c.meijers,f.greco}@tudelft.nl
[2] TeleFlux B.V., Delft, The Netherlands

Abstract. The increasing deployment of Offshore Wind Turbines (OWTs) necessitates larger steel monopiles, whose design currently includes additional steel to account for fatigue damage during installation. Traditional contact-based sensors, such as strain gauges and accelerometers, are challenging to deploy in offshore environments and are susceptible to damage under high stress. To overcome these limitations, a novel non-contact sensor system has been developed, utilizing the magnetomechanical effect to measure strain and an optical method to measure velocity. This paper presents the results of a test series using a full-scale impact hammer on a thin-walled steel pile, comparing the new system's performance to a conventional Pile Driving Analyzer (PDA). Sources of error in the non-contact sensor measurements were identified, and post-processing techniques were applied to obtain acceptable time signals. Despite some residual errors, the system effectively captured strain and velocity behaviour. These findings demonstrate the feasibility of contactless monitoring for steel structures subjected to impact pile driving, representing a promising step toward more efficient and cost-effective monopile installations.

Keywords: non-contact monitoring · impact pile driving · magnetomechanical response · mechanical energy flux

1 Introduction

In the near future, a significant number of Offshore Wind Turbines (OWT) will be installed in offshore locations worldwide [9]. As the capacity and size of these OWTs increase, their foundation piles, usually steel monopiles, also grow larger. Currently, additional steel is required in the design of these monopiles to account for fatigue damage during installation [2]. This excess steel is due to the large safety factors needed, as the fatigue consumption from impact pile driving is not well understood. To reduce this uncertainty and consequently lower the amount of steel used per monopile, it is essential to measure the strain and acceleration of the pile during installation.

Currently, steel structures subjected to dynamic loads are monitored using sensors (such as strain gauges and accelerometers) that must remain in physical

Á. Cunha and E. Caetano (Eds.): EVACES 2025, LNCE 674, pp. 145–153, 2025.
https://doi.org/10.1007/978-3-031-96110-6_12

contact with the structure [1,10]. Attaching and detaching these sensors can be cumbersome, and in offshore environments, it is often practically impossible [8]. Moreover, these sensors are prone to damage when exposed to high stress levels, such as during the impacts of pile driving. A non-contact sensor eliminates these drawbacks, as it does not require physical contact with the structure, making the deployment and redeployment of the sensor more time and cost efficient.

Recently, a non-contact strain measurement system was proposed and validated for steel monopile installations, relying on the magnetic stray field generated by the structure to infer the strains through the magnetomechanical effect [6]. This system was successfully demonstrated during an onshore installation with a hydraulic impact hammer. The system has now been extended to measure the structure's velocity in a non-contact manner as well, allowing for monitoring of the energy flux delivered by the hammer. In this paper, the preliminary results of the performance of this new sensor are presented in terms of accuracy and reliability, by comparing measurements taken during impact hammer tests on an onshore pile to those obtained using a conventional contact-based Pile Driving Analyzer (PDA) under varying hammer blow intensities.

2 Experimental Setup

The impact hammer tests were performed on a steel cylindrical pile which is located at the yard of IQIP in Sliedrecht, the Netherlands. Table 1 summarises the dimensions and material properties of the test pile, in which h denotes the wall thickness, R is the outer radius, and L represents the length of the pile. Moreover, E_p is Young's modulus, ρ_p denotes the density, and ν_p is Poisson's ratio. The impact tests were performed by an S180 hydraulic hammer, which is capable of delivering blows with an impact energy up to 180 kJ.

Table 1. Dimensions and material properties of the steel monopile in Sliedrecht, the Netherlands.

Parameter	Value	Parameter	Value
h	0.050 m	E_p	210 GPa
R	0.6096 m	ρ_p	7850 kg/m^3
L	62.0 m	ν_p	0.3

To measure the axial elastic strain ε_z generated by each hammer impact using a non-contact sensor, the strain-induced magnetic stray field changes in the vicinity of the structure are recorded by a bi-axial magnetometer (type: HMC1022). For the contactless measurement of the axial velocity of the pile v_z, a optical sensor (type: *Measurement Science Enterprise, Inc.* SLV2) is used. This sensor determines the velocity of the pile's surface by processing photographs taken by the internal high-speed camera, yielding the velocity of the plane perpendicular

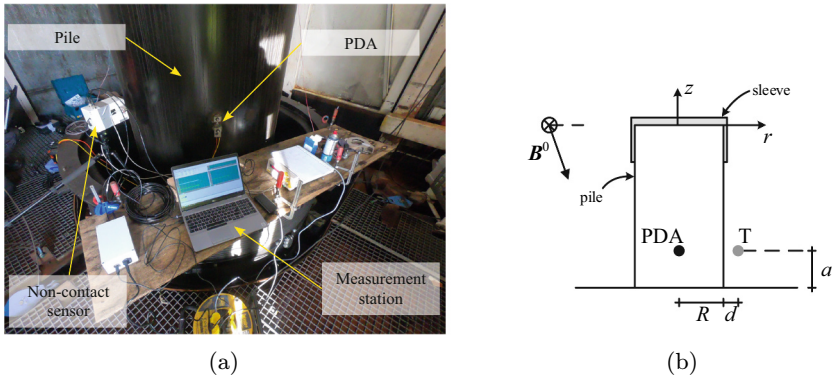

(a) (b)

Fig. 1. Overview of the measurement system during impact hammer tests on the pile. (a) Annotated photograph of the measurement set-up. (b) Schematic view.

to the camera. These two sensors are combined into one box (indicated by T in Fig. 1b), which is connected to a measurement station (Fig. 1a) via a cable. The sensor box containing the non-contact devices is mounted on top of a non-magnetic tripod to ensure that the sensor is placed at a distance $d = 125\,\text{mm}$ (indicated in Fig. 1b) from the surface of the pile.

In parallel to the new contactless sensor, the hammer-induced strains and acceleration are recorded by a conventional Pile Driving Analyser (PDA), which is directly secured to the pile's surface using an adhesive. The PDA consists of a strain measurement device (type: *TML* FLA-2.350-11) and an accelerometer (type: Endevco 7270A) to measure the strain and acceleration in the axial direction, i.e. along the z-axis. All sensors were sampled with a frequency of $F_s = 2\,\text{kHz}$ to correctly capture the dynamic response of the pile to the hammer blows.

3 Data Processing

For each of the sensors described in the previous section, the recorded data is a single time trace, which contains multiple hammer blows. To process the data more efficiently, the entire signal is divided into segments of length $\Delta t = 400\,\text{ms}$, each containing a single hammer blow. Before the data can be compared, certain post-processing has to be performed. For each sensor, the steps are discussed below.

3.1 PDA Data

As the PDA contains two conventional sensors, the post-processing is more straightforward. The PDA directly measures the impact-induced axial strain ε_z. In this paper, contrary to convention, positive values represent compressive strains, while tensile strains are represented by negative values. This reflects

the fact that the hammer blow primarily generated compressive strains in the pile. To remove the high-frequency noise in the measured signal, a low-pass filter with a cutoff frequency of 150 Hz is applied. Figure 2a presents the magnitude response of the applied filter.

The other sensor comprising the PDA measures the axial acceleration a_z. To determine the mechanical energy flux, the axial velocity v_z is of interest, which is determined by integrating the signal once with respect to time. When computing the velocity in this manner, one has to consider the effect of drift, in which the contributions of the measurement noise and a non-zero mean accumulate to yield unrealistic values [7]. Here, this effect is reduced by removing the mean of the acceleration signal before integrating and considering only the small time interval Δt. Then, the same low-pass filter is applied to the velocity signal to remove the remaining high-frequency noise.

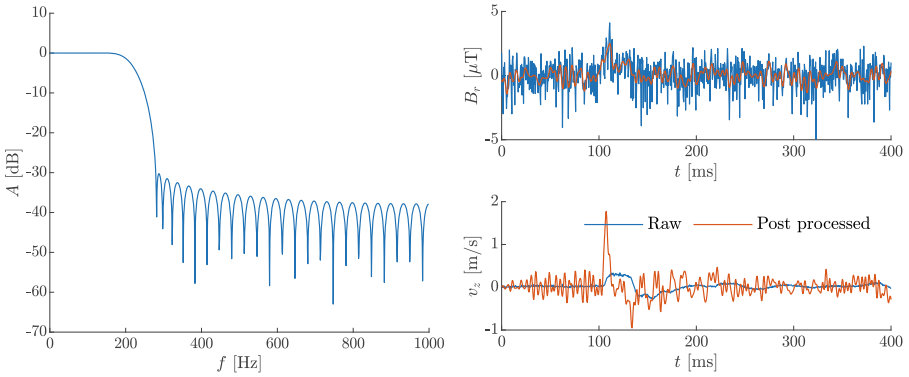

Fig. 2. (a) Characteristics of the low-pass filter. (b) Time series of radial component of the magnetic field (upper) and the axial velocity (lower).

3.2 Contactless Sensor Data

In the case of the contactless sensor, the strain will be inferred from the strain-induced variation of the magnetic stray field of the pile, which is recorded by the magnetic field sensor. As the background magnetic field is time-invariant, the mean of the signal is subtracted from the raw signal. The upper graph in Fig. 2b presents the time series of the dominant component of the magnetic field B_r. The data show that there is a substantial amount of measurement noise contained in the data. Around the time of the hammer blow $t = 100$ ms, there is a peak in the magnetic stray field, which is induced by the strain in the pile. To reduce the effect of the noise, the low-pass filter that was introduced above was applied to the raw data. In the same graph, the post-processed data are

presented. A previous test campaign using a similar magnetic field sensor showed considerably lower noise levels [6], indicating that a better signal-to-noise ratio can be achieved.

For the velocity, the raw data in the lower graph of Fig. 2b show an elongated low peak during the impact. This is the result of the application of a moving average filter inside the firmware of the optical velocity sensor. To obtain the actual velocity signal, the moving average filter needs to be inverted. Unfortunately, this constitutes an ill-posed problem, which means that naively inverting the averaging operator amplifies the measurement noise to such an extent that the data are not representable for the actual signal. Therefore, Tikhonov regularisation is applied to the signal to create a meaningful velocity signal. For each impact, the so-called L-curve is used to determine the optimal value for the regularisation parameter λ [4]. The resulting time trace of the velocity is shown in the same graph. The inversion has successfully reconstructed the peak one expects from a hammer blow. However, a considerable amount of noise is still present in the signal.

4 Results

During the test series, a total of 45 impacts has been recorded. To facilitate the comparison of this number of impacts, the peak value of each time series has been extracted. Since a hammer blow generates a distinct peak in all time series, the peak value provides a way to quantify the response for each variable with a single value. In addition to comparing peak values, the time series of a representable hammer blow will be compared.

4.1 Axial Strain

Before the axial strain signals from both sensors can be compared, the magnetic stray field variation B_r must be converted to axial strain. This conversion is given by

$$\varepsilon_z = C_\varepsilon B_r, \tag{1}$$

in which C_ε is an unknown calibration factor. For each impact, this factor is calculated using the peak value of the strain from the PDA and of the magnetic field. Then, by taking the mean of all 45 impacts, the general conversion factor is determined: $C_\varepsilon = 169\,\mu\varepsilon/\mu\mathrm{T}$. This value will be applied for all impacts.

In Fig. 3a, the upper graph shows the time series of the strain as determined by the two sensors. Despite the high noise level in the contactless sensor's data, the two signals correspond well on the general trends in the signals: a clear peak around $t = 110\,\mathrm{ms}$ and a second smaller peak at $t = 150\,\mathrm{ms}$. To compare all signals, the upper graph in Fig. 3b presents the peak values of the strain obtained by the two sensors. In general, both sensors report the same trend: an increase of peak strain with increasing impact number. The contactless sensor has more fluctuation in the peak value, which can be attributed to the remaining noise in the signal.

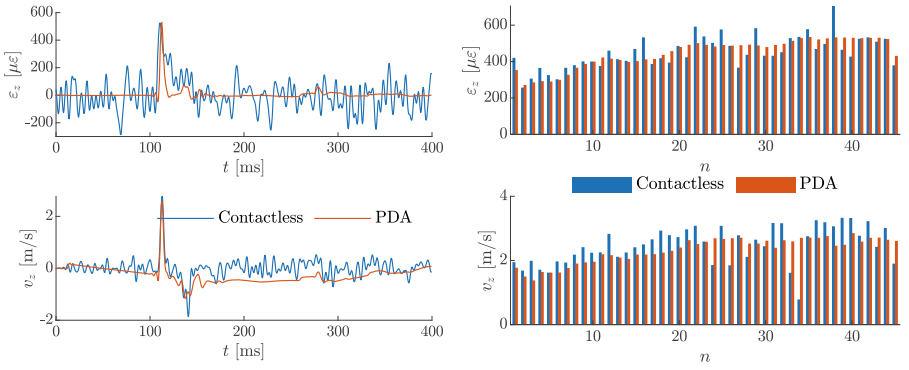

Fig. 3. (a) Time series of the elastic strain (upper) and the axial velocity (lower) of impact 41 as measured by the PDA and contactless sensor. (b) Peak values extracted from all recorded impacts for the elastic strain (upper) and the axial velocity (lower).

4.2 Axial Velocity

In the lower graph in Fig. 3a, the time series of the axial velocity measured by both sensors is presented. Due to the inversion of the moving average filter, the contactless signal shows more fluctuations, which are an artifact from the filter inversion. However, the general trends are well captured. Note that the moving average filter also reduced the peak value for the contactless sensor's data. Therefore, the corrected contactless velocity v_z^{corr} has been scaled such that the peak values of the two signals match by applying

$$v_z^{\text{corr}} = C_v v_z^{\text{pp}}, \tag{2}$$

where v_z^{pp} is the velocity determined by the contactless sensor after the post-processing steps discussed in the previous section. The average numerical value for the correction factor is $C_v = 1.5$, which is applied to the data of all impacts. Important to notice is the drift that is visible in the PDA velocity data even for this short time window. This highlights the importance of directly measuring the velocity instead of relying on acceleration data.

Figure 3b compares the peak values of the velocity in the lower graph. Just as for the strain, the two sensors report the same trend. However, for some impacts, the peak velocity of contactless sensor is much lower than the one of the PDA, e.g. for impact 33 and 34. This might be an artifact of the inversion of the moving average filter. This mismatch and the need for a scaling factor clearly show that the current prototype can be improved to enhance the accuracy and reliability of the velocity measurement.

4.3 Energy Flux and Total Energy

For impact pile driving, the mechanical energy flux in z-direction S_z is given by [3]

$$S_z = 2\pi Rh \left(E_p \varepsilon_z\right) v_z, \tag{3}$$

in which $E_p \varepsilon_z$ represents the uniaxial stress generated by a hammer blow in the pile [5], v_z is the axial velocity, and $2\pi Rh$ denotes the area of the thin-walled pile. Using the energy flux, the total energy E_t that passed through a cross-section of the pile is the determined by an integration with respect to time:

$$E_t = \int S_z \, \mathrm{d}t. \tag{4}$$

The total energy is directly related to the impact energy of the hammer, and it can be used to assess the efficiency of the hammer blows.

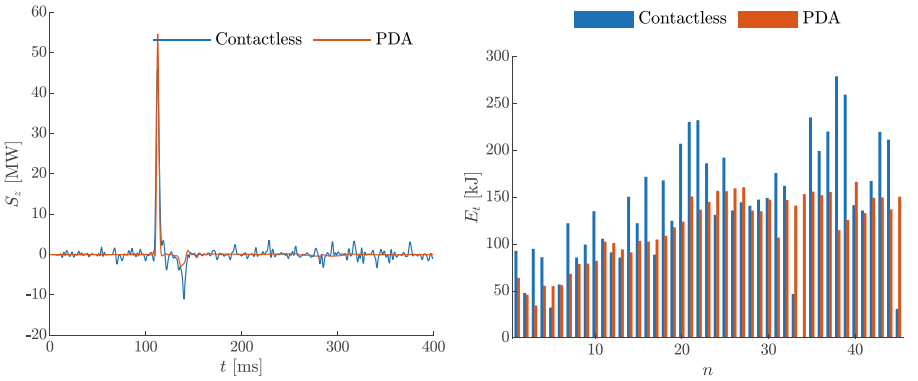

Fig. 4. (a) Time series of the computed energy flux for impact 41. (b) Total energy due to all recorded impacts.

Based on the time series that are presented in Fig. 4a, the computed mechanical energy flux determined by the two sensors can be compared. Again, the two main peaks of the time signal are captured by both sensors. However, the contactless sensor contains much more noise, and the peak value of the two sensors does not correspond. Given the sources of noise reported earlier for the contactless sensors, this is not surprising.

Figure 4b compares the computed total energy for the reported impacts. For this metric, the results of the contactless sensor demonstrate that the current sensors are not accurate enough to represent the actual value, as the contactless value differs almost 50% with the PDA value in some cases. More problematic is the fact that the computed total energy based on the contactless sensor sometimes exceeds the maximal energy the hammer can provide, i.e. 180 kJ. Fortunately, the sources of error for the contactless sensors are known, and they can be addressed in newer versions of the prototype to improve its accuracy and reliability.

5 Conclusions

This paper has reported a test series of impacts on a steel thin-walled pile using a full-scale impact hammer to evaluate the performance of a novel non-contact sensor system for monitoring impact-induced strain and velocity by comparing its measurements to a conventional PDA measurement system. The raw data revealed that the magnetic field sensor exhibited a low signal-to-noise ratio, while the output optical velocity sensor was distorted by a strong smoothing filter. Through post-processing, acceptable time signals were reconstructed. Despite residual errors, the general behaviour of the strain and velocity were well captured. For practical application, improvements in sensor hardware are necessary to enhance the accuracy and reliability of strain and velocity measurements. Nevertheless, the results presented here provide a promising indication that contactless monitoring of mechanical energy flux in steel structures is feasible.

References

1. Buckley RM, Jardine RJ, Kontoe S, Barbosa P, Schroeder FC (2020) Full-scale observations of dynamic and static axial responses of offshore piles driven in chalk and tills. Géotechnique 70(8):657–681. https://doi.org/10.1680/jgeot.19.TI.001
2. Chung J, Wallerand R, Hélias-Brault M (2013) Pile fatigue assessment during driving. Procedia Eng 66:451–463. https://doi.org/10.1016/j.proeng.2013.12.098
3. Gómez SS, Tsetas A, Metrikine AV (2022) Energy flux analysis for quantification of vibratory pile driving efficiency. J Sound Vibr 541:117299
4. Hansen PC (2000) The L-curve and its use in the numerical treatment of inverse problems. In: Johnston P. (ed.) Computational Inverse Problems in Electrocardiology (Advances in Computational Bioengineering). WIT press
5. Meijers PC, Tsouvalas A, Metrikine AV (2018) A non-collocated method to quantify plastic deformation caused by impact pile driving. Int J Mech Sci 148:1–8. https://doi.org/10.1016/j.ijmecsci.2018.08.013
6. Meijers PC, Tsouvalas A, Metrikine AV (2021) Magnetomechanical response of a steel monopile during impact pile driving. Eng Struct 240:112340
7. Smyth A, Wu M (2007) Multi-rate Kalman filtering for the data fusion of displacement and acceleration response measurements in dynamic system monitoring. Mech Syst Sig Process 21(2):706–723

8. Wang P, Tian X, Peng T, Luo Y (2018) A review of the state-of-the-art developments in the field monitoring of offshore structures. Ocean Eng 147:148–164. https://doi.org/10.1016/j.oceaneng.2017.10.014
9. WindEurope (2019) Offshore Wind in Europe. Key trends and statistics. Tech. rep., WindEurope (2020)
10. Wisotzki E, van Foeken R, van Esch P, Novakovic D (2019) Strain and acceleration measurements at instrumentation distances to the pile head of 0.5 and 1.0 times the diameter—offshore pile-monitoring experience. In: Bullock P, Verbeek G, Paikowsky S, Tara D (eds) 10th International Conference on Stress Wave Theory and Testing Methods for Deep Foundations, pp 506–519. ASTM International, West Conshohocken, PA. https://doi.org/10.1520/STP161120170238